Fresnel-Zone Focused Antenna Arrays: Tolerance Analysis for Biomedical Applications

Giovanni Buonanno, *Member, IEEE*, and Sandra Costanzo, *Senior Member, IEEE*

***Abstract*— A detailed tolerance analysis for antenna arrays focused on the Fresnel zone is presented in this work, with the aim to derive the field distribution guaranteeing health safety issues. In particular, random errors related to the amplitudes and phases of the radiators, and random element failures, are considered. As such, the presented tolerance analysis falls within the more prominent theory of random arrays. A particular stochastic function related to the electric field distribution is analyzed and partially characterized by first- and second-order statistics. Subsequently, a discussion is carried out on the estimation of the cumulative distribution function (cdf) for the squared magnitude of the aforementioned random function. This leads to determine (confidence) level curves inherent to the squared magnitude of the electric field, representing a crucial aspect, in particular for safety issues in biomedical applications. The achieved results confirm the validity of the proposed approach, by extending also the literature for far-field focused arrays.**

***Index Terms*— Antenna arrays, biomedical applications, Fresnel zone, health safety, radiative near-field, tolerance analysis.**

I. Introduction

ANTENNA arrays play an extremely important role in a variety of applications, including radar systems, radio astronomy, communication systems, direction finding, electromagnetic heating, medical treatments, microwave imaging [1], [2]. Due to their relevant played role, careful design procedures should be applied. Anyway, even if proceeding with high accuracy approaches, thus adequately fixing, for example, the excitation coefficients and the positions of the elemental radiators, as well as suitably sizing the feeding network to obtain high performance, several error sources can cause the actual electromagnetic field to deviate from the desired one.

Manuscript received 20 March 2023; revised 5 June 2023; accepted 8 July 2023. Date of publication 19 July 2023; date of current version 6 September 2023. This work was supported by the Ministero dell'Università e della Ricerca (MUR), Italy, through "Programma Operativo Nazionale Ricerca e Innovazione 2014–2020" (PON "Ricerca e Innovazione" 2014–2020) Project "Noninvasive Electromagnetic Green Devices and Methods for Advanced Medical Diagnostics." *(Corresponding author: Sandra Costanzo.)*

Giovanni Buonanno is with DIMES, University of Calabria, 87036 Rende, Italy, and also with the Inter-University National Research Center on Interactions between Electromagnetic Fields and Biosystems (ICEmB), 16145 Genoa, Italy (e-mail: giovanni.buonanno@unical.it).

Sandra Costanzo is with DIMES, University of Calabria, 87036 Rende, Italy, also with the National Research Council of Italy (CNR)—Institute for Electromagnetic Sensing of the Environment (IREA), 80124 Naples, Italy, also with the Inter-University National Research Center on Interactions between Electromagnetic Fields and Biosystems (ICEmB), 16145 Genoa, Italy, and also with the Consorzio Nazionale Interuniversitario per le Telecomunicazioni, 43124 Parma, Italy (e-mail: costanzo@dimes.unical.it).

Color versions of one or more figures in this article are available at https://doi.org/10.1109/TAP.2023.3295493.

Digital Object Identifier 10.1109/TAP.2023.3295493

It is generally expensive to realize phased arrays not having amplitude and phase errors [1]. However, even if properly managing the so-called correlated errors [3], the presence of random uncorrelated errors should be properly considered in the design stage, due to their unpredictable nature. For this reason, scientific advances in the tolerance theory of antenna arrays [4] could be strongly beneficial.

To the best of the authors' knowledge, studies involving errors have mostly concerned the far-field of antenna arrays. Indeed, it is worth mentioning the pioneering studies of Ruze [5], Ashmead [7], Gilbert and Morgan [8], Rondinelli [9], Elliott [10], Allen [11], and others [12], [13], [14], [15]. The above studies, even if representing the foundations of the tolerance theory for antenna arrays, are also related to the theory of random arrays [4], leading to deal with the analytical synthesis, in a probabilistic sense, of aperiodic antenna arrays [16], [17]. Excellent discussions on the tolerance theory of far-field focused antenna arrays can be found in [3], [15], and [18]. For the sake of completeness, it is worth mentioning the work in [19], where some results related to antenna arrays in the Fresnel zone, subject to random errors, are presented. The reader may also refer to [20] for a more comprehensive description of the background of the above results.

This work aims to contribute to the analysis of focused antenna arrays in the Fresnel zone, when uncorrelated random errors occur in the amplitude and phase of the excitation coefficients, as well as random element failures may be present. The problem of error characterization in antenna arrays plays a crucial role, as confirmed by the extensive literature at regard. However, most existing works have been focused on the evaluation of the impact the above errors give on the far-field [3], [7], [8], [9], [10], [11], [12], [13], [14], [15], [18], [19], [21], while only a few studies have been addressed to the radiative near-field [20]. This last context is particularly relevant when considering systems designed for security, medical and industrial applications [22], [23]. Thus, the valuable need for the present study can be justified from various perspectives. The first one is that as both the operating frequencies and the physical dimensions of the arrays increase, the relative Fresnel zone becomes more extensive, and therefore the far-field approximation for the electromagnetic field may no longer be valid in the physical region of interest.

An additional, more relevant aspect is that in some applications, such as those occurring in the biomedical context, radiating systems are specifically designed to operate in the

Fresnel zone [20]. Just as an example, Fresnel-zone focusing is of crucial importance in the framework of microwave hyperthermia applications [24], [25]. Here, the field concentration is required into a specific (focal) point where the treatment should be applied, while leaving untouched the surrounding tissues, thus guaranteeing health safety [26]. The Fresnel zone can be also relevant for biomedical implants, using microwaves to recharge [27], [28], [29], [30].

In view of the above considerations, two objectives are pursued in this work. The first one, which turns out to be the incidental one, can be viewed as pedagogical, i.e., to emphasize the link between the tolerance theory and the theory of random arrays, which appear to have been independently developed by scholars, regardless of the observation zone (Fresnel or Fraunhofer) of the antenna array field. The present work basically inherits the methodologies pertinent to the theory of random arrays [16], [35], [36], [37], [38]. It is worth specifying that the errors modeling related to element failures also falls within the scope of the so-called statistically thinned arrays [15], [39], still represented by random arrays [40], [41]. The second objective, the main one, is to extend some existing methodologies for far-field focused arrays in the presence of random errors [18] to the study of focused antenna arrays in the Fresnel zone. For example, the present study may be more attractive in the framework of superficial hyperthermia [26], [27], [28], [29], [30], [31]. In particular, without loss of generality, our analysis is addressed on linear arrays, even if the extension to an arbitrary geometry can be easily performed. Anyway, the choice of linear arrays is coherent with existing literature, such as the study reported in [26], where linear arrays of Antipodal Vivaldi antennas are examined. The most significant concern we are addressing is related to the safety issues regarding the electromagnetic field levels. In particular, the purpose of the present work is to provide a methodology allowing us to predict the behavior of electromagnetic fields in the presence of errors affecting the radiating systems, so to safeguard patients against any high levels of harmful radiation.

Considering a specific function related to the electric field of (Fresnel) focused arrays, a partial first- and second-order statistical characterization is performed. Subsequently, the study of the cumulative distribution function (cdf) of the squared magnitude of the same function is addressed, to determine suitable (confidence) level curves (level surfaces). These curves precisely relate to the levels of squared magnitude of the electric field, to which much attention should be paid in particular applications, such as, for example, those related to the biomedical context. Numerical results are presented and discussed to confirm the validity of the proposed methodology.

II. System Model

Let us consider a linear array of N similar (only complex weights differences are assumed) current densities (antenna elements), immersed into a homogeneous medium, and directed along the z axis of an orthogonal Cartesian reference system, with the relative reference points all arranged along the x axis (Fig. 1). The electric field at a generic point P belonging to the Fresnel (near-field) zone of the above antenna

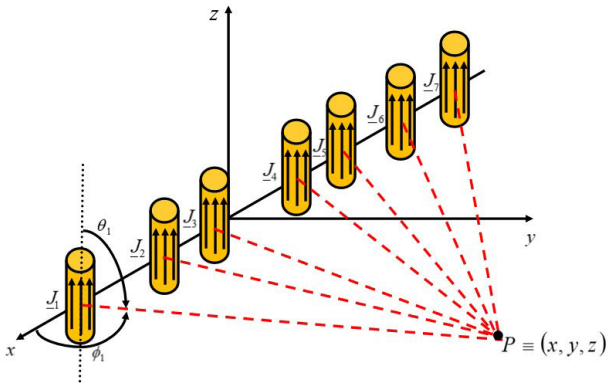

Fig. 1. Array configuration in the Fresnel zone.

array, but placed in the far-field of each array element, can be written as follows:

$$\mathbf{E}(P) = \frac{j\omega\mu}{4\pi}\sum_{n=1}^{N} I_n\,\mathbf{h}_n(P)\,\frac{e^{-jkR_n}}{R_n} \approx \frac{j\omega\mu}{4\pi}\frac{e^{-jkR}}{R}\sum_{n=1}^{N} I_n\mathbf{h}_n(P)e^{jkx_n\sin\theta\cos\phi}e^{-jkx_n^2\frac{\left(1-\sin^2\theta\cos^2\phi\right)}{2R}} \tag{1}$$

where $I_n = A_n\,e^{j\alpha_n}$ is the complex excitation coefficient ($A_n \in \mathbf{R}^+$, $\alpha_n \in [0, 2\pi]$), $k = (2\pi)/\lambda$, λ is the wavelength in the medium, $R_n = \sqrt{(x-x_n)^2 + y^2 + z^2}$, x_n gives the position of the reference point of the nth antenna element, θ and ϕ are the zenithal and azimuthal observation angles, respectively related to the field associated with the entire array, while $\mathbf{h}_n(P)$ is the effective height of the nth antenna element, given as follows:

$$\begin{aligned}\mathbf{h}_n(P) &= \hat{\boldsymbol{\theta}}_n\,\sin\theta_n \times \int_{x'}\int_{y'}\int_{z'}\Big\{J\left(x', y', z'\right) \times e^{jk\left(x'\sin\theta_n\cos\phi_n + y'\sin\theta_n\sin\phi_n + z'\cos\theta_n\right)}\Big\}\,dx'dy'dz' \\ &= h_n(\theta_n, \phi_n)\,\hat{\boldsymbol{\theta}}_n.\end{aligned} \tag{2}$$

In the above expression, $\mathbf{J}(x, y, z) = J(x, y, z)\,\hat{\mathbf{z}}$ is the current density taken as a reference for all elements. Accordingly, $\mathbf{J}_n(x, y, z) = I_n\,J(x, y, z)\,\hat{\mathbf{z}}$ for the nth element. Moreover, θ_n and ϕ_n are the observation angles of the field associated with the nth element. Of course, θ_n and ϕ_n can be seen as functions of θ and ϕ and also of x_n. As regarding the phases $\{\phi_n\}_{n=1}^N$, they can be chosen in such a way to realize a focusing in correspondence with the focal point (R_f, θ_f, ϕ_f) [4]. Therefore, in this case, we have

$$\alpha_n = -kx_n\sin\theta_f\cos\phi_f + kx_n^2\frac{1-\sin^2\theta_f\cos^2\phi_f}{2R_f} - \angle\,h_n\left(\theta_{n_f}, \phi_{n_f}\right) \tag{3}$$

where θ_{n_f} and ϕ_{n_f} are the values assumed by angles θ_n and ϕ_n when $\theta = \theta_f$ and $\phi = \phi_f$. Moreover, for the sake of clarity, as well as to give more emphasis on the geometric and parametric properties of the array in the Fresnel zone, let us

assume that: the directivity diagram of all antenna elements reaches its maximum for $\theta = \pi/2$; the focal point is located in the xy plane ($\theta_f = \pi/2$); let us observe the field in the same plane ($\theta = \pi/2 \Rightarrow \theta_n = \pi/2$ and $\hat{\boldsymbol{\theta}}_n = \hat{\boldsymbol{\theta}} = -\hat{\mathbf{z}}\ \forall\ n$), thereby studying a mathematical model similar to that in [19] and [42] (antenna arrays in Fresnel zone), in [4] (continuous sources in Fresnel zone). It is worth highlighting that this setting approach is also similar to that considered for the so-called *array factor in near field* [2], where the focal point is also in the xy plane, and the observation is made in the same plane. Furthermore, it must be considered that for directions $\theta \neq 0$, the directivity effects of the antenna elements also begin to be felt. Therefore, the function to be studied is given by the following expression:

$$\begin{aligned}&\mathbf{E}(R, \pi/2, \phi)\\ &= \frac{j\omega\mu}{4\pi}\frac{e^{-jkR}}{R}\sum_{n=1}^{N} I_n\, h_n(\pi/2, \phi_n)\, e^{jkx_n\cos\phi}\, e^{-jkx_n^2\frac{\sin^2\phi}{2R}}\left(-\hat{\mathbf{z}}\right)\\ &= \frac{j\omega\mu}{4\pi}\frac{e^{-jkR}}{R}F(R, \phi)\left(-\hat{\mathbf{z}}\right)\end{aligned} \tag{4}$$

deducing that, in this case, it is possible to study a simplified scalar problem, gathering attention to the function $F(R, \phi)$. For the sake of simplicity, this function is hereinafter referred to the "*radiation function*."

Now, let us suppose that during the (real-time) operation of the system, the following conditions hold true: 1) the amplitudes and phases of the excitation coefficients are subject to errors due to the mutual coupling and fluctuations in the power supply network and 2) antenna elements can fail with a given probability. Furthermore, the tolerances of the feeding network components must be also considered. Consequently, the actual version of the function $F(R, \phi)$ can be modeled, more realistically, as follows [$h_n = h_n(\pi/2, \phi_n)$]:

$$\begin{aligned}&\widetilde{F}(R, \phi)\\ &= \sum_{n=1}^{N}\Big\{(A_n + \delta A_n)\, F_n\, e^{j(\alpha_n+\delta\alpha_n)}\, h_n\\ &\qquad\times e^{jk\,x_n\cos\phi}\, e^{-jk\,x_n^2\frac{\sin^2\phi}{2R}}\Big\}\\ &= \sum_{n=1}^{N}\Big\{(A_n + \delta A_n)\, F_n|h_n|\\ &\qquad\times\cos\left(kx_n\cos\phi - kx_n^2\frac{sin^2\phi}{2R} + \alpha_n + \delta\alpha_n + \angle h_n\right)\Big\}\\ &\quad + j\sum_{n=1}^{N}\Big\{(A_n + \delta A_n)\, F_n|h_n|\\ &\qquad\times\sin\left(kx_n\cos\phi - kx_n^2\frac{sin^2\phi}{2R} + \alpha_n + \delta\alpha_n + \angle h_n\right)\Big\}\\ &= \widetilde{F}_{\mathcal{R}}(R, \phi) + j\,\widetilde{F}_{\mathcal{I}}(R, \phi)\end{aligned} \tag{5}$$

where $\widetilde{F}_{\mathcal{R}}(R, \phi)$ and $\widetilde{F}_{\mathcal{I}}(R, \phi)$ are the real and the imaginary part of the radiation function, respectively. By referring to the tolerance theory of antenna arrays (in the far-field) [3], [4], [15], here it is assumed that $\{F_n\}_{n=1}^N$, $\{\delta A_n\}_{n=1}^N$, $\{\delta\alpha_n\}_{n=1}^N$ are all independent random variables. More precisely, in a similar way as [18], it is assumed that $\{\delta A_n\}_{n=1}^N$ are continuous independent random variables with zero mean but, in general, with different variance (i.e., $\overline{\delta A_n} = 0\ \forall\ n$ and $\sigma^2_{\delta A_n} = \overline{\delta A_n^2} \neq \sigma^2_{\delta A_m} = \overline{\delta A_m^2}$ for $n \neq m$); the same holds for $\{\delta\alpha_n\}_{n=1}^N$ ($\overline{\delta\alpha_n} = 0\ \forall\ n$, $\sigma^2_{\delta\alpha_n} = \overline{\delta\alpha_n^2} \neq \sigma^2_{\delta\alpha_m} = \overline{\delta\alpha_m^2}$ for $n \neq m$; instead, as regards $\{F_n\}_{n=1}^N$, they are modeled as independent identically distributed (i.i.d.) binary random variables ($\overline{F_n} = p$ and $F_n \in \{0, 1\}\ \forall\ n$). Therefore, it follows that $\widetilde{F}(R, \phi)$ is a stochastic process to be studied by means of probability theory. It is worth mentioning that the considered errors are the most common ones [3].

In the following, some implicit results are initially presented for (5), in the sense that no particular geometry for radiators is considered (i.e., $\{h_n(\theta_n, \phi_n)\}_{n=1}^N$ are left implicit). Subsequently, reference is made to dipole arrays, and then the results are properly specialized to this type of geometry for the antenna elements. It is worth emphasizing that this approach does not invalidate the generality of the presented methodology, since the directivity of the antenna elements is a deterministic function, and therefore it does not affect the various statistical properties that are analyzed.

An important point must be further highlighted. In the model given by (5), the mutual couplings are assumed to be weak enough so not to change the vector structure and the shape of the current densities (or fields) on the radiators, leading all antenna elements to share the same radiation pattern. More specifically, it is assumed that the mutual couplings can only influence the values of the input currents of the radiators, and such effects are implicitly taken into account through the errors related to the excitation coefficients, even if in a simplified way.

III. Partial Characterization of the Actual Radiation Function

A. Mean Characteristics of the Actual Radiation Function

The mean of the actual radiation function $\widetilde{F}(R, \phi)$ is given as follows:

$$\begin{aligned}&\mu(R, \phi)\\ &= \overline{\widetilde{F}(R, \phi)}\\ &= \sum_{n=1}^{N}\overline{(A_n+\delta A_n)}\,\overline{F_n}\, e^{j\alpha_n}\,\overline{e^{j\delta\alpha_n}}\, h_n(\pi/2, \phi_n)\, e^{jkx_n\cos\phi}\, e^{-jkx_n^2\frac{\sin^2\phi}{2R}}\\ &= p\sum_{n=1}^{N} A_n e^{j\alpha_n} h_n(\pi/2, \phi_n)\, e^{-\frac{\sigma^2_{\delta\alpha_n}}{2}}\, e^{jkx_n\cos\phi}\, e^{-jkx_n^2\frac{\sin^2\phi}{2R}}\end{aligned} \tag{6}$$

in which it has been assumed that the phase errors are *zero-mean* Gaussian random variables [15], [18], i.e., $\overline{e^{j\delta\alpha_n}} = e^{-(\sigma^2_{\delta\alpha_n}/2)}$, taking into account that $\sigma^2_{\delta\alpha_n}$ is the variance of the nth phase error. As can be seen, amplitude errors do not affect the mean radiation function, whereas phase errors and element failures do. In particular, these two errors imply lower values for the magnitude of the mean of the actual radiation function with respect to the ideal case [i.e., with respect to $F(R, \phi)$]. One way to overcome this disadvantage could be to multiply $\widetilde{F}(R, \phi)$ by a real constant that compensates for the aforementioned decrease.

In addition to the mean of the radiation function, it is very useful to observe the behavior of the mean of the squared magnitude of $\widetilde{F}(R,\phi)$, which is associated with the radiated power density, given by (with $h_n(\pi/2,\phi_n)=h_n$)

$$\begin{aligned}
&\overline{\left|\widetilde{F}(R,\phi)\right|^2}\\
&=\sum_{n=1}^{N}\sum_{m=1}^{N}\Bigg\{\overline{(A_n+\delta A_n)\,(A_m+\delta A_m)}\;\overline{F_n\,F_m}\;e^{j(\alpha_n-\alpha_m)}\\
&\qquad\times\overline{e^{j(\delta\alpha_n-\delta\alpha_m)}}\;h_n\,h_m^*\,e^{jk(x_n-x_m)\cos\phi}\,e^{-jk\left(x_n^2-x_m^2\right)\frac{\sin^2\phi}{2R}}\Bigg\}\\
&=|F(R,\phi)|^2+\sum_{n=1}^{N}\sum_{m=1}^{N}\Bigg\{A_n\,A_m\,e^{j(\alpha_n-\alpha_m)}\,e^{jk(x_n-x_m)\cos\phi}\\
&\qquad\times e^{-jk\left(x_n^2-x_m^2\right)\frac{\sin^2\phi}{2R}}\,h_n\,h_m^*\\
&\qquad\times\left[\overline{F_n\,F_m}\;\overline{e^{j(\delta\alpha_n-\delta\alpha_m)}}-1\right]\Bigg\}\\
&\quad+\sum_{n=1}^{N}\sum_{m=1}^{N}\Bigg\{\overline{\delta A_n\,\delta A_m}\;\overline{F_n\,F_m}\;e^{j(\alpha_n-\alpha_m)}\;\overline{e^{j(\delta\alpha_n-\delta\alpha_m)}}\;h_n h_m^*\\
&\qquad\times e^{jk(x_n-x_m)\cos\phi}\,e^{-jk\left(x_n^2-x_m^2\right)\frac{\sin^2\phi}{2R}}\Bigg\}\\
&=|F(R,\phi)|^2+\sum_{n=1}^{N}\left\{A_n^2\,|h_n|^2\,(p-1)\right\}+\sum_{n=1}^{N}\left\{\sigma_{\delta A_n}^2\,p\,|h_n|^2\right\}\\
&\quad+\sum\sum_{n\neq m}\Bigg\{A_n\,A_m\,e^{j(\alpha_n-\alpha_m)}\,e^{jk(x_n-x_m)\cos\phi}\\
&\qquad\times e^{-jk\left(x_n^2-x_m^2\right)\frac{\sin^2\phi}{2R}}\,h_n\,h_m^*\left[p^2\,e^{-\frac{\sigma_{\delta\alpha_n}^2+\sigma_{\delta\alpha_m}^2}{2}}-1\right]\Bigg\}
\end{aligned}\tag{7}$$

taking into account that, in this framework, $F_n^2=F_n\;\forall\;n$ and $\overline{\delta A_n^2}=\sigma_{\delta A_n}^2$ is the variance of the nth amplitude error. As can be seen, random errors are responsible for the appearance of numerous (error) terms in addition to the squared magnitude of the desired radiation function.

B. Variance of the Actual Radiation Function

The statistical mean of the actual radiation function is not related to specific realizations of random errors, but it rather describes the behavior of the above function averaged over a very large number of statistical realizations of the errors. Hence, there is a need to obtain more information regarding even a generic sample path of $\widetilde{F}(R,\phi)$. The variance is a statistical metric that can contribute to this, being related to the average distance that the various sample paths of the radiation function exhibit with respect to the mean. Thus, the variance of $\widetilde{F}(R,\phi)$ is given as follows:

$$\begin{aligned}
&\sigma^2(R,\phi)\\
&=\overline{\left|\widetilde{F}(R,\phi)-\mu(R,\phi)\right|^2}\\
&=\overline{\left|\widetilde{F}(R,\phi)\right|^2}-\left|\overline{\widetilde{F}(R,\phi)}\right|^2\\
&=p\sum_{n=1}^{N}\left[\left(A_n^2+\overline{\delta A_n^2}\right)|h_n|^2\right]-p^2\sum_{n=1}^{N}\left[A_n^2|h_n|^2\left|\overline{e^{j\delta\alpha_n}}\right|^2\right]\\
&=\sum_{n=1}^{N}\left\{p\,A_n^2|h_n|^2\left[1-p\,e^{-\sigma_{\delta\alpha_n}^2}\right]\right\}+\sum_{n=1}^{N}\left[p\,\sigma_{\delta A_n}^2|h_n|^2\right].
\end{aligned}\tag{8}$$

Observing (8), it is interesting to note that the variance of the radiation function does not depend on the distance from the origin of the reference system, i.e., it does not depend on R, while it depends on the azimuthal observation angle, ϕ, through the angles $\{\phi_n\}_{n=1}^N$.

C. Characterization of the Real and Imaginary Parts of the Actual Radiation Function

In order to perform an in-depth analysis, it is also advantageous to statistically characterize the real and imaginary parts of the radiation function. In particular, the functions $\widetilde{F}_{\mathcal{R}}(R,\phi)$ and $\widetilde{F}_{\mathcal{I}}(R,\phi)$ are first analyzed separately, and then their covariance is also taken into account.

The mean and variance of $\widetilde{F}_{\mathcal{R}}(R,\phi)$ are given as follows:

$$\begin{aligned}
&\mu_{\mathcal{R}}(R,\phi)\\
&=\overline{\widetilde{F}_{\mathcal{R}}(R,\phi)}\\
&=p\sum_{n=1}^{N}\Bigg\{A_n|h_n|\\
&\qquad\times\overline{\cos\left[kx_n\cos\phi-kx_n^2\frac{\sin^2\phi}{2R}+\alpha_n+\delta\alpha_n+\angle h_n\right]}\Bigg\}\\
&=p\sum_{n=1}^{N}\Bigg\{A_n e^{-\frac{\sigma_{\delta\alpha_n}^2}{2}}|h_n|\\
&\qquad\times\cos\left[kx_n\cos\phi-kx_n^2\frac{\sin^2\phi}{2R}+\alpha_n+\angle h_n(\pi/2,\phi_n)\right]\Bigg\}
\end{aligned}\tag{9}$$

$$\begin{aligned}
&\sigma_{\mathcal{R}}^2(R,\phi)\\
&=\overline{\widetilde{F}_{\mathcal{R}}^2(R,\phi)}-\mu_{\mathcal{R}}^2(R,\phi)\\
&=\frac{p}{2}\sum_{n=1}^{N}\Bigg\{\left(A_n^2+\sigma_{A_n}^2\right)|h_n|^2\,e^{-2\sigma_{\delta\alpha_n}^2}\\
&\qquad\times\cos\left[2kx_n\cos\phi-2kx_n^2\frac{\sin^2\phi}{2R}+2\alpha_n+\angle h_n\right]\Bigg\}\\
&\quad+\frac{p}{2}\sum_{n=1}^{N}\left(A_n^2+\sigma_{A_n}^2\right)|h_n|^2-\frac{p^2}{2}\sum_{n=1}^{N}A_n^2|h_n|^2e^{-\sigma_{\delta\alpha_n}^2}\\
&\quad-\frac{p^2}{2}\sum_{n=1}^{N}\Bigg\{A_n^2|h_n|^2e^{-\sigma_{\delta\alpha_n}^2}\\
&\qquad\times\cos\left[2kx_n\cos\phi-2kx_n^2\frac{\sin^2\phi}{2R}+2\alpha_n+2\angle h_n\right]\Bigg\}.
\end{aligned}\tag{10}$$

The mean and variance of $\widetilde{F}_{\mathcal{I}}(R,\phi)$ can be written as follows:

$$\mu_{\mathcal{I}}(R,\phi)=\overline{\widetilde{F}_{\mathcal{R}}(R,\phi)}$$

$$= p\sum_{n=1}^{N}\Bigg\{A_n|h_n| \times \overline{\sin\left[kx_n\cos\phi - kx_n^2\frac{\sin^2\phi}{2R} + \alpha_n + \delta\alpha_n + \angle h_n(\pi/2,\phi_n)\right]}\Bigg\}$$

$$= p\sum_{n=1}^{N}\Bigg\{A_n\, e^{-\frac{\sigma_{\delta\alpha_n}^2}{2}}|h_n| \times \sin\left[kx_n\cos\phi - kx_n^2\frac{\sin^2\phi}{2R} + \alpha_n + \angle h_n(\pi/2,\phi_n)\right]\Bigg\} \tag{11}$$

$$\begin{aligned}\sigma_{\mathcal{I}}^2(R,\phi) &= \overline{\widetilde{F}_{\mathcal{I}}^2(R,\phi)} - \mu_{\mathcal{I}}^2(R,\phi)\\ &= -\frac{p}{2}\sum_{n=1}^{N}\Bigg\{\left(A_n^2+\sigma_{A_n}^2\right)|h_n|^2\, e^{-2\sigma_{\delta\alpha_n}^2} \times \cos\Bigg[2kx_n\cos\phi - 2kx_n^2\frac{\sin^2\phi}{2R} + 2\alpha_n + \angle h_n(\pi/2,\phi_n)\Bigg]\Bigg\}\\ &\quad + \frac{p}{2}\sum_{n=1}^{N}\left(A_n^2+\sigma_{A_n}^2\right)|h_n|^2 - \frac{p^2}{2}\sum_{n=1}^{N}A_n^2|h_n|^2 e^{-\sigma_{\delta\alpha_n}^2}\\ &\quad + \frac{p^2}{2}\sum_{n=1}^{N}\Bigg\{A_n^2|h_n|^2 e^{-\sigma_{\delta\alpha_n}^2} \times \cos\left[2kx_n\cos\phi - 2kx_n^2\frac{\sin^2\phi}{2R} + 2\alpha_n + 2\angle h_n\right]\Bigg\}.\end{aligned} \tag{12}$$

At this point, it is advantageous to consider the following two cases: 1) the analysis of the behavior of $\widetilde{F}(R,\phi)$ as a function of ϕ for $R = R_f$ and 2) the analysis of the behavior of $\widetilde{F}(R,\phi)$ as a function of R for $\phi = \phi_f$.

Observing the expressions of $\mu_{\mathcal{R}}(R,\phi)$ and $\mu_{\mathcal{I}}(R,\phi)$, we note that, if each α_n is given by (3), at $R = R_f$ and $\phi = \phi_f$ the function $\mu_{\mathcal{R}}(R,\phi)$ assumes the maximum value while $\mu_{\mathcal{I}}(R,\phi)$ is equal to zero. Instead, for $R \neq R_f$ and/or $\phi \neq \phi_f$, $\mu_{\mathcal{R}}(R,\phi)$ and $\mu_{\mathcal{I}}(R,\phi)$ are given by "incoherent" sums of cosines and sines, respectively. Consequently, looking at $\mu_{\mathcal{R}}(R,\phi)$ and $\mu_{\mathcal{I}}(R,\phi)$ as only functions of ϕ and for $R = R_f$, in the region of the main-lobe and near-in side-lobes, $\mu_{\mathcal{I}}(R,\phi)$ assumes negligible values with respect to $\mu_{\mathcal{R}}(R,\phi)$. Instead, in the region away from the main-lobe, $\mu_{\mathcal{R}}(R,\phi)$ and $\mu_{\mathcal{I}}(R,\phi)$ have almost the same values. This aspect is all the more valid the higher the number of antenna elements, as it can be seen from Fig. 2, in which $|\mu_{\mathcal{R}}(R_f,\phi)|$ and $|\mu_{\mathcal{I}}(R_f,\phi)|$ are shown as the number of antenna elements varies, for $\theta_f = \pi/2$, $\phi_f = \pi/2$ and $R_f = (R_{min} + R_{MAX})/2$, with $R_{min} = 0.62\sqrt{L^3/\lambda}$ (lower boundary of the Fresnel zone), $R_{MAX} = 2(L^2/\lambda)$ (upper boundary of the Fresnel zone), $L = (N-1)(\lambda/2)$ (array aperture), $x_{n+1} - x_n = \lambda/2\ \forall\, n$ (half-wavelength spacing), and where the antenna elements are short dipoles. For each n: $A_n = 1$ V, $\sigma_{\delta A_n} = 0.1$ V, $\sigma_{\delta\alpha_n} = 0.1$ rad and $p_n = 0.97$. Furthermore, for the construction of the diagrams the normalization with respect to Δz, i.e., with respect to the length of the generic short dipole, has been considered (that is, the behavior of $F(R,\phi)/\Delta z$ has been observed).

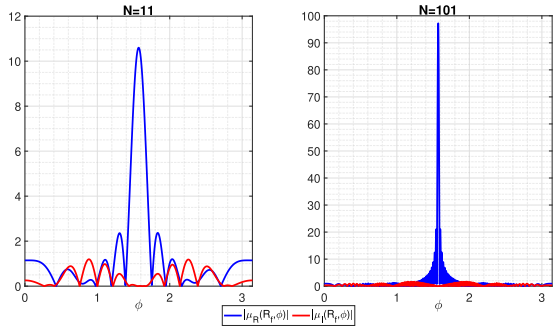

Fig. 2. Magnitudes of $\mu_{\mathcal{R}}(R,\phi)$ and $\mu_{\mathcal{I}}(R,\phi)$ as functions of ϕ for $R = R_f$, as the number of antenna elements varies.

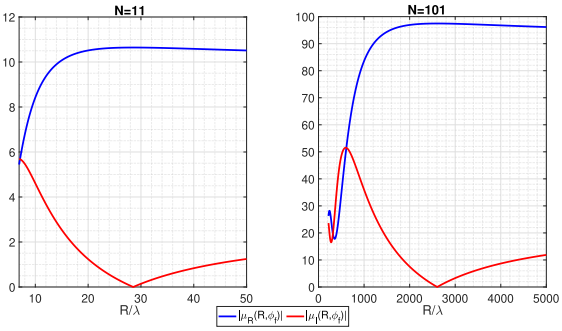

Fig. 3. Magnitudes of $\mu_{\mathcal{R}}(R,\phi)$ and $\mu_{\mathcal{I}}(R,\phi)$ as functions of R for $\phi = \phi_f$, as the number of antenna elements varies.

Fig. 3 shows the behaviors of $|\mu_{\mathcal{R}}(R,\phi)|$ and $|\mu_{\mathcal{I}}(R,\phi)|$ as a function of R for $\phi = \phi_f$. In this case, even if no main-lobe and side-lobes appear along R the radiation function, it can be observed that in the neighborhood of the focal point the function $\mu_{\mathcal{I}}(R,\phi)$ assumes increasingly negligible values with respect to $\mu_{\mathcal{R}}(R,\phi)$ as the number of elements increases.

Figs. 4 and 5 show the standard deviations along ϕ (for $R = R_f$) and along R (for $\phi = \phi_f$), respectively, as the number of antenna elements varies. As can be seen, along ϕ the standard deviations take on significantly different values at the ends of the observation interval and in correspondence with the focal point, while at the other point they have almost the same values. And, as can be seen, this aspect is more pronounced as the number of elements increases. This is consistent with what is shown in the literature regarding the study of the far-field of antenna arrays [18]. Indeed, for $R = R_f$, the radiation function behaves similar to the array factor *focused* at $\phi = \phi_f$. As regards the behavior of the standard deviations along R, also in this case there is a substantial difference since $\sigma_{\mathcal{R}}(R,\phi_f)$ and $\sigma_{\mathcal{I}}(R,\phi_f)$ are different throughout the observation interval.

Now, let us study the (linear) correlation between the quadrature components of the radiation function. Thus, the covariance function between the real and imaginary parts of the radiation function must be considered, namely

$$\mathcal{K}(R,\phi) = \overline{\widetilde{F}_{\mathcal{R}}(R,\phi)\,\widetilde{F}_{\mathcal{I}}(R,\phi)} - \mu_{\mathcal{R}}(R,\phi)\,\mu_{\mathcal{I}}(R,\phi)$$

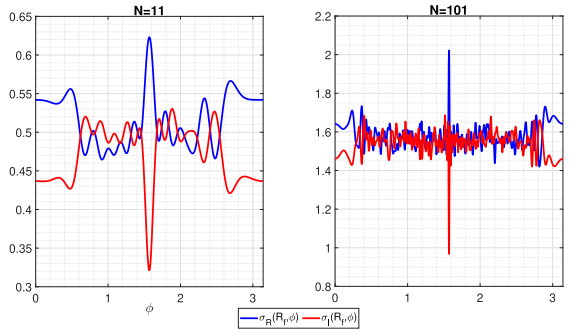

Fig. 4. Standard deviations of the real and imaginary parts of the radiation function as functions of ϕ for $R = R_f$, as the number of antenna elements varies.

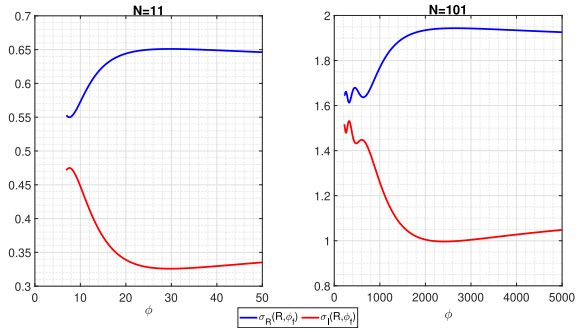

Fig. 5. Standard deviations of the real and imaginary parts of the radiation function as functions of R for $\phi = \phi_f$, as the number of antenna elements varies.

$$= \sum_{n=1}^{N} \left\{ \frac{p}{2} |h_n|^2 \, e^{-\sigma^2_{\delta\alpha_n}} \left[\left(A_n^2 + \sigma^2_{\delta A_n} \right) e^{-\sigma^2_{\delta\alpha_n}} - p\, A_n^2 \right] \times \sin\left[2kx_n \cos\phi - 2kx_n^2 \frac{\sin^2\phi}{2R} + 2\alpha_n + 2\angle h_n \right] \right\} \quad (13)$$

which leads to the Bravais-Pearson correlation coefficient $\rho(R,\phi) = \mathcal{K}(R,\phi)/[\sigma_{\mathcal{R}}(R,\phi)\,\sigma_{\mathcal{I}}(R,\phi)]$. Figs. 6 and 7 show the behavior of the correlation coefficient with the same array settings as in the previous figures. In particular, Fig. 6 shows the behavior of the correlation coefficient as a function of the azimuthal variable ϕ (and for $R = R_f$) for different values of N. As can be seen, except for a few points of the observation interval, $\rho(R_f,\phi)$ assumes increasingly smaller values as the number of elements increases. Fig. 7, on the other hand, shows the behavior of the correlation coefficient as a function of R/λ, for $\phi = \phi_f$. In this case, although the correlation coefficient takes on relatively low values, it is not entirely negligible even as the number of elements increases. However, it can be observed that it crosses the zero level with a positive slope for $R \approx R_f$, regardless of the number of elements, keeping low values around this point.

Therefore, it can be observed that the quadrature components of the (actual) radiation function are asymptotically (with respect to N) uncorrelated for $R = R_f$, while, more generally, they can be assumed to be uncorrelated around the focal point.

It is worth highlighting that the obtained results could be quite easily generalized to the case in which the field is observed in points not belonging to the xy plane.

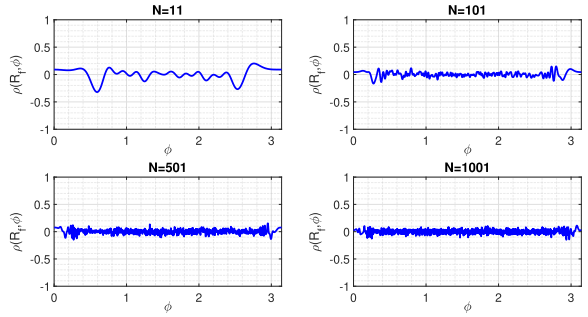

Fig. 6. Correlation coefficient between the real and imaginary parts of $\widetilde{F}(R,\phi)$ as a function of ϕ for $R = R_f$, as the number of antenna elements varies.

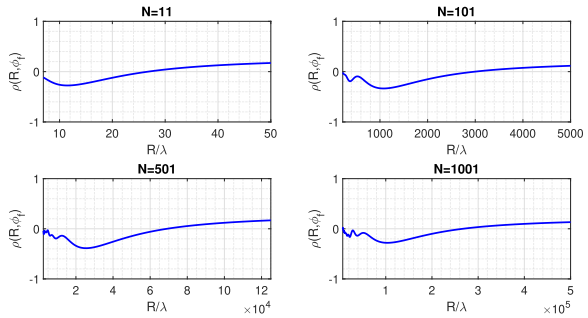

Fig. 7. Correlation coefficient between the real and imaginary parts of $\widetilde{F}(R,\phi)$ as a function of R for $\phi = \phi_f$, as the number of antenna elements varies.

IV. Distribution of the Squared Magnitude of the Actual Radiation Function

So far, the obtained analytic results do not depend on the number of antenna elements. Instead, when the number of radiators is high enough for the validity of the (multivariate) central limit theorem (CLT) [43], it is possible to have a more accurate description of the radiation function behavior. Indeed, the real and imaginary parts of the radiation function can be seen as asymptotically (with respect to N) jointly Gaussian. Accordingly, their joint probability density function (pdf) can be written as (with (R,ϕ) implied)

$$f\left(\widetilde{F}_{\mathcal{R}}, \widetilde{F}_{\mathcal{I}}\right) = \frac{e^{-\frac{1}{2(1-\rho^2)}\left[\frac{(\widetilde{F}_{\mathcal{R}}-\mu_{\mathcal{R}})^2}{\sigma^2_{\mathcal{R}}} - 2\rho\,\frac{(\widetilde{F}_{\mathcal{R}}-\mu_{\mathcal{R}})}{\sigma_{\mathcal{R}}}\,\frac{(\widetilde{F}_{\mathcal{I}}-\mu_{\mathcal{I}})}{\sigma_{\mathcal{I}}} + \frac{(\widetilde{F}_{\mathcal{I}}-\mu_{\mathcal{I}})^2}{\sigma^2_{\mathcal{I}}}\right]}}{2\pi\,\sigma_{\mathcal{R}}\,\sigma_{\mathcal{I}}\sqrt{1-\rho^2}} \quad (14)$$

and therefore the distribution of the squared magnitude of the radiation function, $P(R,\phi) = |\widetilde{F}(R,\phi)|^2$, is given by

$$\mathcal{P}_r\left\{P(R,\phi) \le \xi^2\right\} = \int\int_{\left|\widetilde{F}(R,\phi)\right|^2 \le \xi^2} f\left(\widetilde{F}_{\mathcal{R}}, \widetilde{F}_{\mathcal{I}}\right) d\widetilde{F}_{\mathcal{R}}\, d\widetilde{F}_{\mathcal{I}} \quad (15)$$

for which, to the best of the authors' knowledge, there is no closed-form representation.

A. General Approach

This section proposes a general approach to obtain a lower bound on the distribution of $P(R,\phi)$. Referring to (14), it is possible to write [44]

$$\iint_A f\left(\widetilde{F}_{\mathcal{R}}, \widetilde{F}_{\mathcal{I}}\right) d\widetilde{F}_{\mathcal{R}}\, d\widetilde{F}_{\mathcal{I}} = 1 - e^{-\frac{a^2}{2}} \quad (16)$$

in which A is the area included within the ellipse of the following equation (with R and ϕ implied):

$$\frac{\left(\widetilde{F}_{\mathcal{R}}-\mu_{\mathcal{R}}\right)^2}{\sigma_{\mathcal{R}}^2}-2\,\rho\,\frac{\left(\widetilde{F}_{\mathcal{R}}-\mu_{\mathcal{R}}\right)}{\sigma_{\mathcal{R}}}\,\frac{\left(\widetilde{F}_{\mathcal{I}}-\mu_{\mathcal{I}}\right)}{\sigma_{\mathcal{I}}}+\frac{\left(\widetilde{F}_{\mathcal{I}}-\mu_{\mathcal{I}}\right)^2}{\sigma_{\mathcal{I}}^2}=a^2\left(1-\rho^2\right) \quad (17)$$

whose center is the point (μ_x, μ_y), whose major radius is $a\sqrt{\tau_{MAX}}$, whose minor radius is $a\sqrt{\tau_{min}}$, with τ_{MAX} and τ_{min} being the largest and smallest eigenvalues of the covariance matrix, respectively [45]. The parameter a coincides with the Mahalanobis distance of the point $(\widetilde{F}_{\mathcal{R}}, \widetilde{F}_{\mathcal{I}})$ from the above bivariate Gaussian distribution [45]. Consequently, through (16)–(17) it is possible to determine a lower-bound for (15). Indeed, if the smallest circle centered in $(\widetilde{F}_{\mathcal{R}}, \widetilde{F}_{\mathcal{I}}) = (0, 0)$ and encompassing the aforementioned ellipse is considered, then it is possible to write that

$$\mathcal{P}_r\left\{P(R,\phi)\le\xi^2\right\}\ge 1-e^{-\frac{a^2}{2}} \quad (18)$$

in which ξ is precisely the radius of the circle. Thus, considering an "extreme" case, if the area A is such that $(1-e^{-(a^2/2)})\to 100\%$, then (18) becomes approximately an equality. Also, from the same (18), it can be obtained a lower bound for the parameter a. In fact, it can be written that (with $\mathcal{P}_r \equiv \mathcal{P}_r\{P(R,\phi)\le\xi^2\}$)

$$a\ge\sqrt{-2\,\ln\left(1-\mathcal{P}_r^2\right)}. \quad (19)$$

Now, one last piece is missing, i.e., the determination of the radius of the smallest circle which encompasses the ellipse and is, therefore, tangent to this last one. To do this, the following parametric representation of the ellipse can be exploited [45] (with (R, ϕ) implied):

$$\begin{cases}\widetilde{F}_{\mathcal{R}}=a\,\sigma_{\mathcal{R}}\,\cos t+\mu_{\mathcal{R}}\\ \widetilde{F}_{\mathcal{I}}=a\,\sigma_{\mathcal{I}}\left[\rho\,\cos t+\sqrt{1-\rho^2}\,\sin t\right]+\mu_{\mathcal{I}}\end{cases} \quad (20)$$

in which $t\in[0,2\pi]$. The variable ξ represents the radius of the above smallest circle, which is

$$\xi=\max_t\left\{\sqrt{\widetilde{F}_{\mathcal{R}}^2+\widetilde{F}_{\mathcal{I}}^2}\right\},\quad t\in[0,2\pi]. \quad (21)$$

The above expressions can be useful for estimating the punctual [namely, for fixed (R, ϕ)] percentiles of $P(R, \phi)$. In fact, the $\eta\%$ level curve (in general, level surface) $r_\eta(R, \phi)$ (with $0 \le \eta \le 100$), which is such that $\mathcal{P}_r\{P(R,\phi) \le r_\eta(R,\phi)\} = \eta\%$, can be achieved first by setting $\mathcal{P}_r = \eta\%$; then, by determining the Mahalanobis distance a with the assumption that (19) is equality; afterward, by computing $\widetilde{F}_{\mathcal{R}}$ and $\widetilde{F}_{\mathcal{I}}$ as functions of t by means of (20); finally, by reckoning the radius ξ through (21), taking into account that, in this circumstance, $r_\eta(R,\phi)\approx\xi$ for the generic point (R, ϕ).

For the sake of completeness, it is worth noting that Chebyshev inequality can also be exploited in the following way:

$$\mathcal{P}_r\left\{\left|P(R,\phi)-\overline{P(R,\phi)}\right|<\xi\,\sigma_P(R,\phi)\right\}\ge 1-\frac{1}{\xi^2} \quad (22)$$

where $\overline{P(R,\phi)}=\overline{|\widetilde{F}(R,\phi)|^2}$, while $\sigma_P(R,\phi)$ is the standard deviation of the $P(R,\phi)$, which can be written as [38] (with R and ϕ implied)

$$\sigma_P^2(R,\phi)=4\mu_{\mathcal{R}}^2\sigma_{\mathcal{R}}^2+4\mu_{\mathcal{I}}^2\sigma_{\mathcal{I}}^2+2\sigma_{\mathcal{R}}^4+2\sigma_{\mathcal{I}}^4-\mu_{\mathcal{R}}^2\mu_{\mathcal{I}}^2-\mu_{\mathcal{R}}^2\sigma_{\mathcal{I}}^2-\mu_{\mathcal{I}}^2\sigma_{\mathcal{R}}^2-\sigma_{\mathcal{R}}^2\sigma_{\mathcal{I}}^2+2\mathcal{K}\left[\mathcal{K}+2\mu_{\mathcal{R}}\mu_{\mathcal{I}}\right]. \quad (23)$$

Moreover, exploiting the Dharmadhikari result [47], it is possible to obtain bounds for the percentile surface

$$\begin{aligned}&\overline{P(R,\phi)}-\sigma_P(R,\phi)\sqrt{\frac{1-\eta\%}{\eta\%}}\\ &\quad\le r_\eta(R,\phi)\\ &\quad\le\overline{P(R,\phi)}+\sigma_P(R,\phi)\sqrt{\frac{\eta\%}{1-\eta\%}}.\end{aligned} \quad (24)$$

It is worth highlighting that in case the field is observed in points not belonging to the xy plane, it is possible to generalize the presented approach considering a multivariate normal density [45] and therefore dealing with hyperellipsoids and hyperspheres.

Finally, for the sake of clarity, it is worth specifying that $\widetilde{F}_{\mathcal{R}}$ and $\widetilde{F}_{\mathcal{I}}$ appearing in (14)–(17) and (20)–(21) are not the quadrature components of $\widetilde{F}(R,\phi)$ but variables associated with them. The same symbols have been used to denote different quantities in order not to overburden the notation. The same holds for the other distributions that are presented below.

B. Study of the Distribution of $|F(R,\phi)|$ as Function of ϕ for $R = R_f$

So far, the results seen for the distribution of $P(R,\phi)$ are general, in the sense that they hold for any point (R,ϕ). However, for the particular cases that are shown below, it is possible to exploit the arguments of the theory of random arrays [16], [38] and of the tolerance theory of far-field focused arrays [3], [12], [18].

Let us analyze the behavior of $\mathcal{P}_r\{P(R,\phi)\le\xi^2\}$ for $R = R_f$. In this case, it has been seen that the correlation coefficient is (asymptotically) negligible; therefore the quadrature components of the radiation function can be assumed to be independent. Accordingly, the distribution of $P(R,\phi)$ can be approximated as follows:

$$\begin{aligned}&\mathcal{P}_r\left\{P\left(R_f,\phi\right)\le\xi^2\right\}\\ &=\int_{-\xi}^{\xi}\left\{\left[Q\left(\frac{-\sqrt{\xi^2-\widetilde{F}_{\mathcal{R}}^2}-\mu_{\mathcal{I}}}{\sigma_{\mathcal{I}}}\right)-Q\left(\frac{\sqrt{\xi^2-\widetilde{F}_{\mathcal{R}}^2}-\mu_{\mathcal{I}}}{\sigma_{\mathcal{I}}}\right)\right]\times\frac{e^{-\frac{\left(\widetilde{F}_{\mathcal{R}}-\mu_{\mathcal{R}}\right)^2}{2\sigma_{\mathcal{R}}^2}}}{\sqrt{2\pi}\,\sigma_{\mathcal{R}}}\right\}d\widetilde{F}_{\mathcal{R}}\end{aligned} \quad (25)$$

with $Q(z)=(1/\sqrt{2\pi})\int_z^\infty e^{-t^2/2}dt$ being the Q-function [44]. It is worth noting that, by suitable manipulations such as those in [48], it is possible to attain closed-form representations of the Q-functions with very limited approximation errors [44].

However, as can be seen, (25) still requires numerical integration, given that, as far as the authors are aware, not even for it there exists a closed-form representation, though some approximations can be found in [17]. However, as it has been shown previously, as N increases, the standard deviations of $F_{\mathcal{R}}(R_f,\phi)$ and $F_{\mathcal{I}}(R_f,\phi)$ become similar to each other, except for a limited portion of the domain of ϕ. Consequently, when $\sigma_{\mathcal{I}}(R_f,\phi)\approx\sigma_{\mathcal{R}}(R_f,\phi)$, $P(R_f,\phi)/\sigma_{\mathcal{R}}(R_f,\phi)$ becomes a non-central χ-square random variables with two degrees of freedom at point (R_f,ϕ), thus being able to write

$$\mathcal{P}_r\left\{\frac{P\left(R_f,\phi\right)}{\sigma^2_{\mathcal{R}}\left(R_f,\phi\right)}\le\xi^2\right\}\approx 1-\mathrm{Q}_1\left(\frac{\left|\mu\left(R_f,\phi\right)\right|}{\sigma_{\mathcal{R}}\left(R_f,\phi\right)},\xi\right) \quad (26)$$

in which $Q_1(a,b)$ is the Marcum Q-function of order 1 [49] and $|\mu(R_f,\phi)|$ is determined by means (6). This is a result that can be found in random array theory [38] and implicitly also in the tolerance theory for arrays in far-field [3]. Also, following [38], it is possible to determine the following $\eta\%$ level curve of $P(R_f,\phi)/\sigma^2_{\mathcal{R}}(R_f,\phi)$ (with R_f and ϕ implied):

$$\begin{aligned}&\mathcal{LC}^2_\eta\left(R_f,\phi\right)\\&\approx\left(2+\frac{|\mu|^2}{\sigma^2_{\mathcal{R}}}\right)\\&\quad\times\left[\nu_\eta\sqrt{\frac{4}{9}\frac{\left(|\mu|^2\sigma^2_{\mathcal{R}}+\sigma^4_{\mathcal{R}}\right)}{\left(|\mu|^2+2\sigma^2_{\mathcal{R}}\right)^2}}+1-\frac{4}{9}\frac{\left(|\mu|^2\sigma^2_{\mathcal{R}}+\sigma^4_{\mathcal{R}}\right)}{\left(|\mu|^2+2\sigma^2_{\mathcal{R}}\right)^2}\right]^3\end{aligned} \quad (27)$$

in which ν_η is the ηth percentile of the standardized Gaussian random variable. Thus, for the generic point (R_f,ϕ), the value of $\mathcal{LC}^2_\eta(R_f,\phi)$ represents the approximate ηth percentile of $P(R_f,\phi)/\sigma^2_{\mathcal{R}}(R_f,\phi)$, without recurring to any inversion. What is more, the function $\mathcal{LC}^2_\eta(R_f,\phi)$, for $\phi\in[0,2\pi]$, represents a level curve for $P(R_f,\phi)/\sigma^2_{\mathcal{R}}(R_f,\phi)$. Accordingly, in this case the estimate of the function $r_\eta(R_f,\phi)$ is $\mathcal{LC}^2_\eta(R_f,\phi)\times\sigma^2_{\mathcal{R}}(R_f,\phi)$.

Finally, at points where even $\mu_{\mathcal{R}}(R_f,\phi)$ and $\mu_{\mathcal{I}}(R_f,\phi)$ can be considered negligible (with respect to $\sigma_{\mathcal{R}}(R_f,\phi)$ and $\sigma_{\mathcal{I}}(R_f,\phi)$, respectively), the distribution of $P(R_f,\phi)/\sigma^2_{\mathcal{R}}(R,\phi)$ becomes

$$\mathcal{P}_r\left\{\frac{P\left(R_f,\phi\right)}{\sigma^2_{\mathcal{R}}\left(R_f,\phi\right)}\le\xi^2\right\}\approx 1-e^{-\frac{\xi^2}{2}}. \quad (28)$$

C. Behavior of the cdf of $|F(R,\phi)|$ Along R for $\phi=\phi_f$

As it has been shown, along R the behaviors of the quadratures components of $F(R,\phi)$ do not allow to arrive at a relation similar to (26). Furthermore, also the correlation coefficient between $F_{\mathcal{R}}(R,\phi_f)$ and $F_{\mathcal{I}}(R,\phi_f)$ is not entirely negligible even as the number of antenna elements increases. Consequently, also in this case it is necessary to refer to the more general results given by (16)–(19).

V. Characterization of the Error Between the Actual Radiation Function and the Ideal One

The variance given by (8) is a distance metric that exists between the sample paths and the mean of $\widetilde{F}(R,\phi)$. However, the mean of $\widetilde{F}(R,\phi)$ does not represent the ideal radiation function $F(R,\phi)$. As a matter of fact, this is contained into (4). For this reason, it is more appropriate to measure instead the distance between $F(R,\phi)$ and $\widetilde{F}(R,\phi)$, considering the stochastic process $\epsilon(R,\phi)=\widetilde{F}(R,\phi)-F(R,\phi)$. Accordingly, it is possible to calculate the following mean squared error:

$$\begin{aligned}\mathrm{MSE}(R,\phi)&=\overline{|\epsilon(R,\phi)|^2}\\&=\overline{\left|\widetilde{F}(R,\phi)-F(R,\phi)\right|^2}\\&=\overline{\left|\widetilde{F}(R,\phi)\right|^2}-2\,\Re\left\{\mu(R,\phi)\,F^*(R,\phi)\right\}\\&\quad+|F(R,\phi)|^2\\&=|\mu(R,\phi)|^2+\sigma^2(R,\phi)\\&\quad-2\,\Re\left\{\mu(R,\phi)\,F^*(R,\phi)\right\}+|F(R,\phi)|^2\end{aligned} \quad (29)$$

in which $\Re\{\mu(R,\phi)\,F^*(R,\phi)\}$ is the real part of $\mu(R,\phi)\,F^*(R,\phi)$ and the symbol * stands for complex conjugation.

It is worth highlighting that, referring to the results presented in Section IV, a deeper characterization of the stochastic process $\epsilon(R,\phi)$ can be performed. In fact, it is possible to apply the same arguments for determining the cdf of the magnitude of $\epsilon(R,\phi)$. In this case, (14) has to be modified in order to obtain the joint pdf between the real and the imaginary parts of $\epsilon(R,\phi)$ (with R and ϕ implied), namely

$$\begin{aligned}&f(\epsilon_{\mathcal{R}},\epsilon_{\mathcal{I}})\\&=\frac{e^{-\frac{1}{2\left(1-\rho^2\right)}\left[\frac{(\epsilon_{\mathcal{R}}-\mu_{\mathcal{R}}+F_{\mathcal{R}})^2}{\sigma^2_{\mathcal{R}}}-2\rho\frac{(\epsilon_{\mathcal{R}}-\mu_{\mathcal{R}}+F_{\mathcal{R}})}{\sigma_{\mathcal{R}}}\frac{(\epsilon_{\mathcal{I}}-\mu_{\mathcal{I}}+F_{\mathcal{I}})}{\sigma_{\mathcal{I}}}+\frac{(\epsilon_{\mathcal{I}}-\mu_{\mathcal{I}}+F_{\mathcal{I}})^2}{\sigma^2_{\mathcal{I}}}\right]}}{2\pi\sigma_{\mathcal{R}}\sigma_{\mathcal{I}}\sqrt{1-\rho^2}}\end{aligned} \quad (30)$$

where $F_{\mathcal{R}}(R,\phi)$ and $F_{\mathcal{I}}(R,\phi)$ are the real and the imaginary parts of $F(R\phi)$. Accordingly, the following ellipse equation is associated to (30):

$$\begin{aligned}&\frac{(\epsilon_{\mathcal{R}}-\mu_{\mathcal{R}}+F_{\mathcal{R}})^2}{\sigma^2_{\mathcal{R}}}-2\,\rho\,\frac{(\epsilon_{\mathcal{R}}-\mu_{\mathcal{R}}+F_{\mathcal{R}})}{\sigma_{\mathcal{R}}}\frac{(\epsilon_{\mathcal{I}}-\mu_{\mathcal{I}}+F_{\mathcal{I}})}{\sigma_{\mathcal{I}}}\\&\qquad+\frac{(\epsilon_{\mathcal{I}}-\mu_{\mathcal{I}}+F_{\mathcal{I}})^2}{\sigma^2_{\mathcal{I}}}=a^2\left(1-\rho^2\right)\end{aligned} \quad (31)$$

and therefore, referring to (18), in this case, the variable ξ represents the radius of the smallest circle which contains the ellipse given by (31). Therefore, by proceeding in a similar way as with (16)–(21), it is possible to obtain a lower bound for the cdf of $|\epsilon(R,\phi)|^2$.

Then, studying $\epsilon(R,\phi)$ as a function of ϕ and for $R=R_f$, it is possible to assume $\rho\approx 0$ and therefore, referring to (25), we can write

$$\begin{aligned}\mathcal{P}_r\left\{\left|\epsilon\left(R_f,\phi\right)\right|^2\le\xi^2\right\}&=\int_{-\xi}^{\xi}d\epsilon_{\mathcal{R}}\,\frac{e^{-\frac{(\epsilon_{\mathcal{R}}-\mu_{\mathcal{R}}+F_{\mathcal{R}})^2}{2\sigma^2_{\mathcal{R}}}}}{\sqrt{2\pi}\,\sigma_{\mathcal{R}}}\\&\quad\times\left[Q\left(\frac{-\sqrt{\xi^2-\epsilon^2_{\mathcal{R}}}-\mu_{\mathcal{I}}+F_{\mathcal{I}}}{\sigma_{\mathcal{I}}}\right)\right.\\&\quad\left.-Q\left(\frac{\sqrt{\xi^2-\epsilon^2_{\mathcal{R}}}-\mu_{\mathcal{I}}+F_{\mathcal{I}}}{\sigma_{\mathcal{I}}}\right)\right].\end{aligned} \quad (32)$$

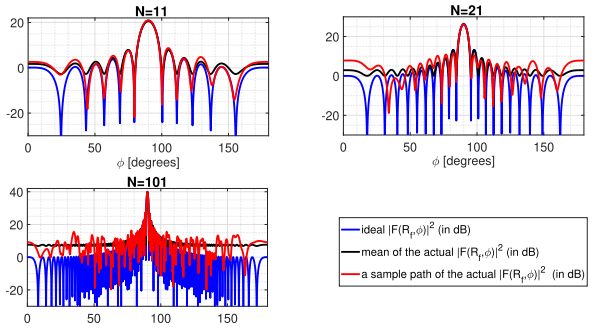

Fig. 8. Comparison of the squared magnitude of $F(R,\phi)$ (blue line), the mean squared magnitude of $\widetilde{F}(R,\phi)$ (black line), and the squared magnitude of a sample path of $\widetilde{F}(R,\phi)$ (red line), for $R=R_f$, as the number of antenna elements varies. Each function is in dB.

Again, at points where $\rho(R_f,\phi)\approx 0$ and $\sigma_{\mathcal{I}}(R_f,\phi)\approx\sigma_{\mathcal{R}}(R_f,\phi)$, the function $|\epsilon(R_f,\phi)|^2/\sigma^2_{\mathcal{R}}(R_f,\phi)$ is a non-central χ-squared random variable and its ηth percentile is given by

$$\widetilde{\mathcal{LC}^2_\eta}(R_f,\phi) \approx \left(2+\frac{a^2}{\sigma^2_{\mathcal{R}}}\right)\left[\nu_\eta\sqrt{\frac{4}{9}\frac{\left(a^2\sigma^2_{\mathcal{R}}+\sigma^4_{\mathcal{R}}\right)}{\left(a^2+2\sigma^2_{\mathcal{R}}\right)^2}}+1-\frac{4}{9}\frac{\left(a^2\sigma^2_{\mathcal{R}}+\sigma^4_{\mathcal{R}}\right)}{\left(a^2+2\sigma^2_{\mathcal{R}}\right)^2}\right]^3 \tag{33}$$

in which $a^2=\{[\mu_{\mathcal{R}}(R_f,\phi)-F_{\mathcal{R}}(R_f,\phi)]^2+[\mu_{\mathcal{I}}(R_f,\phi)-F_{\mathcal{I}}(R_f,\phi)]^2\}$.

VI. Numerical Results

In this section, some significant examples are shown to validate the previous arguments. As before, we consider arrays of short dipoles for computational convenience, without loss of generality. Indeed, it is worth noting that the reported theoretical results do not depend on the type of antenna chosen for the array. Also, the focal point is given as $(R_f,\theta_f,\phi_f)=([0.62\sqrt{L^3/\lambda}+2\,(L^2/\lambda)]/2,\pi/2,\pi/2)$ and for each n: $A_n=1$ V, $x_{n+1}-x_n=\lambda/2$, $\sigma_{\delta A_n}=0.1$ V, $\sigma_{\delta\alpha_n}=0.1$ rad, and $p_n=0.97$.

Fig. 8 is inherent to the behavior of $F(R,\phi)$ and $\widetilde{F}(R,\phi)$ along ϕ, for $R=R_f$ and different values of the antenna elements. In particular, this figure shows the behaviors of the squared magnitude of $F(R_f,\phi)$, the mean squared magnitude of $\widetilde{F}(R_f,\phi)$ and the squared magnitude of a realization (sample path) of the same $\widetilde{F}(R_f,\phi)$. As can be seen, for low values (case $N=11$) of the number of elemental radiators these three functions show quite superimposable trends. Instead, as this number increases, the curves gradually separate from each other (case $N=21$). This can be observed quite markedly for the case $N=101$. Indeed, the squared magnitude of $F(RF,\phi)$ decreases as the values of ϕ move away from ϕ_f, similar to what happens for far-field focused arrays; instead, the mean squared magnitude of $\widetilde{F}(R_f,\phi)$ shows a main-lobe superimposable on that of $|F(R_f,\phi)|^2$ but then an almost constant level in the (*pseudo*) sidelobe region, similar to what occurs for far-field focused random arrays [4]; finally, the generic sample path of $|\widetilde{F}(R_f,\phi)|^2$ is almost similar to that of the other two functions in the region containing the main-lobe and near-in side-lobes, while it has a noisy behavior for ϕ values far from the main-lobe, once again similar to what occurs for far-field focused random arrays [4].

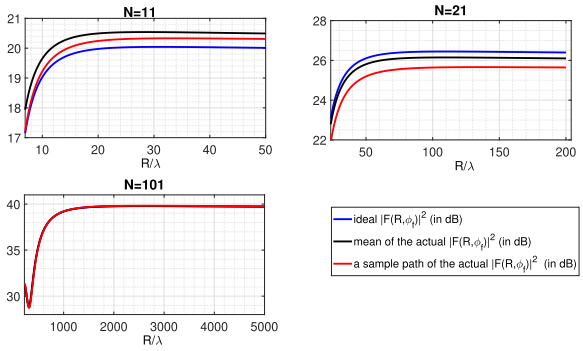

Fig. 9. Comparison of the magnitude of $F(R,\phi)$ (blue line), the mean squared magnitude of $\widetilde{F}(R,\phi)$ (black line), and the magnitude of a sample path of $\widetilde{F}(R,\phi)$ (red line), for $\phi=\phi_f$, as the number of antenna elements varies. Each function is in dB.

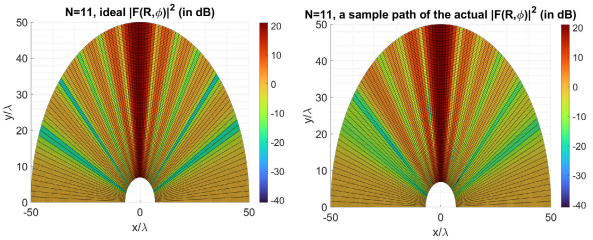

Fig. 10. Comparison between the magnitude of $F(R,\phi)$ and the magnitude of a sample path of $\widetilde{F}(R,\phi)$, in the whole Fresnel domain, for $N=11$.

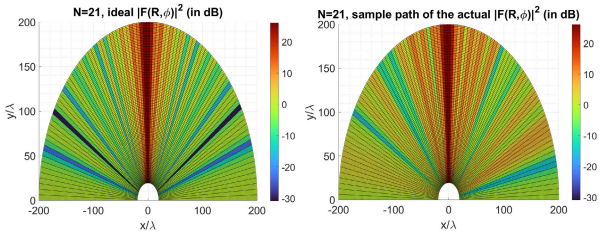

Fig. 11. Comparison between the magnitude of $F(R,\phi)$ and the magnitude of a sample path of $\widetilde{F}(R,\phi)$ in the whole Fresnel domain, for $N=21$.

Fig. 9 shows the behavior of $|F(R,\phi)|^2$, $|\widetilde{F}(R,\phi)|^2$ and a sample path of $|\widetilde{F}(R,\phi)|^2$ along R for $\phi=\phi_f$. In this case, contrary to Fig. 8, the deviation between the various curves gradually becomes less marked as the number of radiators increases.

The previous figures allow us to obtain only a partial view of the functions under examination. For this reason, in Figs. 10–12 the trends of $|F(R,\phi)|^2$ and $|\widetilde{F}(R,\phi)|^2$ are globally taken into consideration, i.e., in the whole Fresnel zone of the array under consideration. These figures confirm that the squared magnitude of the sample path of $|\widetilde{F}(R,\phi)|$ globally presents higher levels than those related to the squared magnitude of $F(R,\phi)$.

Now, let us evaluate the performance of the estimates of the *cdf* of $P(R,\phi)$. Fig. 13 shows the mean and a sample path of $|\widetilde{F}(R_f,\phi)|^2$ along with the empirical 99% level curve, obtained by Monte Carlo analysis, and the theoretical 99%

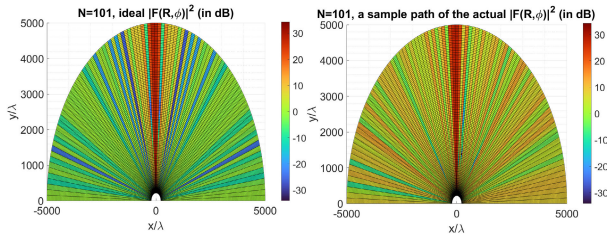

Fig. 12. Comparison between the magnitude of $F(R,\phi)$ and the magnitude of a sample path of $\widetilde{F}(R,\phi)$ in the whole Fresnel domain, for $N=101$.

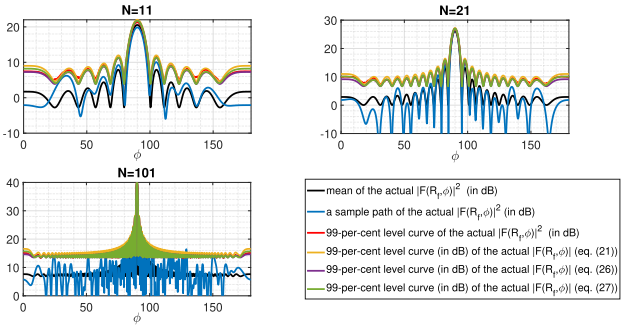

Fig. 13. Mean and level curves of $|\widetilde{F}(R_f,\phi)|^2$ in dB, as the number of antenna elements varies.

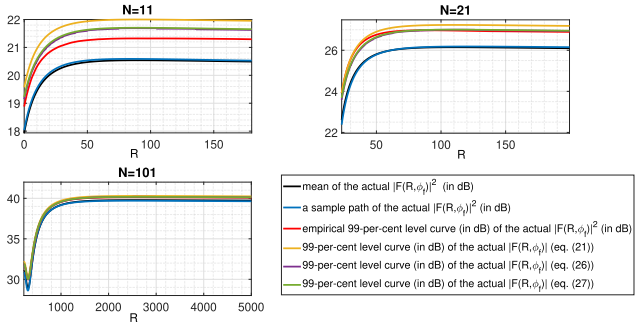

Fig. 14. Mean and level curves of $|\widetilde{F}(R,\phi_f)|^2$ in dB, as the number of antenna elements varies.

level curves obtained through the approaches of Section IV, as the number of antenna elements varies. Considering the 99% level curves helps provide a *margin of safety* especially when the arrays are used, for example, in biomedical scenarios. As can be seen, the theoretical level curves provide a good estimate even for low values of the number of radiators. In fact, it is worth noting that they are based on the Gaussianity assumption between the quadrature component of $\widetilde{F}(R,\phi)$, which in turn is based on the multivariate CLT. Therefore, even for such a small number of elements, it is possible to obtain a good estimate of the level curves by exploiting the aforementioned Gaussianity assumption. *A fortiori*, this methodology can be used to study the performance of large arrays in their Fresnel zone. However, as it is possible to observe, the results are also valid in the case of arrays composed of a moderate number of elements. Indeed, the methodology shown was positively tested also for $N=11$.

Fig. 14 shows the same functions as in Fig. 13 this time along R for $\phi=\phi_f$. As can be seen, again there is a good matching between the empirical 99% level curve and the theoretical ones.

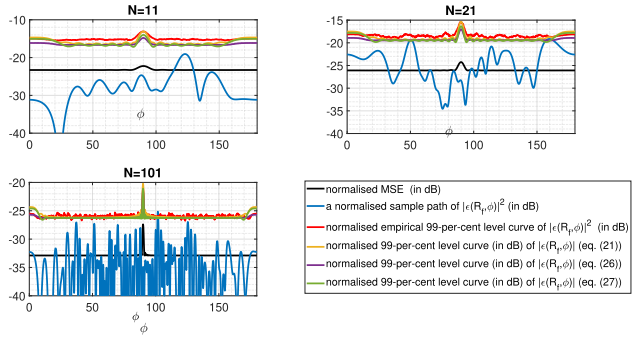

Fig. 15. Mean and level curves of $|\epsilon(R,\phi_f)|^2$ in dB, as the number of antenna elements varies. All curves are normalized with respect to the supremum of the mean of the squared magnitude of $\widetilde{F}(R_f,\phi)$.

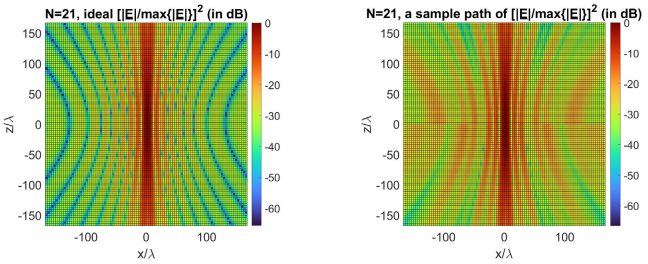

Fig. 16. Comparison between the error-free and actual normalized magnitude squared of the electric field, in dB, in the plane parallel to the xz plane and positioned at $y=R_f$, having dimensions $[-\sqrt{R_{MAX}^2-R_f^2},\sqrt{R_{MAX}^2-R_f^2}]\times[-\sqrt{R_{MAX}^2-R_f^2},\sqrt{R_{MAX}^2-R_f^2}]$.

Finally, for greater completeness, Fig. 15 also provides an analysis relating to the error function $\epsilon(R,\phi)$. In particular, this figure compares the function $MSE(R,\phi)$, given by (29), a realization of $|\epsilon(R,\phi)|^2$ and the 99% level curves associated with the latter, along ϕ for $R=R_f$. These functions are all normalized with respect to the supremum of $|\widetilde{F}(R_f,\phi)|^2$, so that the 99% level curves represent a sort of estimate of the (pseudo) peak sidelobe level of $|\widetilde{F}(R_f,\phi)|$. As becomes evident, also in this case the theoretical level curves provide a good estimate of the true (empirical) one. Furthermore, it is worth noting that as the number of elements increases, the levels of the sample paths of $|\epsilon(R,\phi)|$ decrease, and with it also the levels of the related functions, thus indicating that the impact of errors decreases. This is similar to what occurs for random (far-field focused) arrays [38].

Finally, to have a complete view of the performance of the arrays under investigation, Fig. 16 compares the behavior of the errors-free and actual electric field magnitudes in the plane parallel to the xz plane and placed at $y=R_f$. The highest field values are obtained around the focal point, but, again, it can be observed that the effect of errors translates into a general rise in field levels.

VII. Conclusion

A tolerance analysis applied to Fresnel-zone focused antenna arrays has been presented in this work, with the aim to predict the field levels and guarantee safety issues in biomedical contexts. In particular, amplitude, phase, and fault errors have been considered, which are modeled as usual

in terms of independent random variables. Consequently, the proposed methodology can also be regarded as an important topic in the framework of random array theory. As a primary objective, the work has been intended to study the near-field randomness, by providing relationships to predict the levels (i.e., confidence curves/surfaces) related to the stochastic electromagnetic field both in range and azimuth. The study has been primarily motivated to face the problem of arrays errors in most common biomedical applications, such as hyperthermia and implants recharging. Numerical results on linear arrays have been discussed to confirm the validity of the proposed approach, which can be easily extended to arbitrary array geometries.

Finally, it has been assumed that mutual couplings could only modify the excitation coefficients of the array, but leaving unchanged the current distribution (or field) on the radiators. In a simplified way, their influence has been taken into account through the errors related to the excitation coefficients. Anyway, the presence of mutual couplings in antenna arrays represents a serious problem, and future studies will be addressed to accurately take them into account also in the case of antenna arrays focused in the Fresnel-zone.

REFERENCES

[1] N. Fourikis, *Advanced Array Systems, Applications and RF Technologies* (Signal Processing and its Applications), 1st ed. New York, NY, USA: Academic, 2000.

[2] R. L. Haupt, *Antenna Arrays: A Computational Approach*. Hoboken, NJ, USA: Wiley, 2010.

[3] R. J. Mailloux, *Phased Array Antenna Handbook*, 2nd ed. Norwood, MA, USA: Artech House, 2005.

[4] B. D. Steinberg, *Principles of Aperture and Array System Design*. New York, NY, USA: Wiley, 1976.

[5] J. Ruze, "Physical limitations on antennas," M.S. thesis, Dept. Elect. Eng., Massachusetts Inst. Technol., Cambridge, MA, USA, May 1952.

[6] J. Ruze, "Antenna tolerance theory—A review," *Proc. IEEE*, vol. 54, no. 4, pp. 633–640, Apr. 1966.

[7] D. Ashmead, "Optimum design of linear arrays in the presence of random errors," *Trans. IRE Prof. Group Antennas Propag.*, vol. 4, no. 1, pp. 81–92, Dec. 1952.

[8] E. N. Gilbert and S. P. Morgan, "Optimum design of directive antenna arrays subject to random variations," *Bell Syst. Tech. J.*, vol. 34, no. 3, pp. 637–663, May 1955.

[9] L. A. Rondinelli, "Effects of random errors on the performance of antenna arrays of many elements," in *Proc. IRE Nat. Conv. Rec.*, 1959, pp. 174–189.

[10] R. Elliott, "Mechanical and electrical tolerances for two-dimensional scanning antenna arrays," *IRE Trans. Antennas Propag.*, vol. 6, no. 1, pp. 114–120, Jan. 1958.

[11] J. L. Allen, "Some extensions of the theory of random error effects on array patterns," in *Phased Array Radar Studies*. Nov. 1961, ch. 3.

[12] J. K. Hsiao, "Array sidelobes, error tolerance, gain, and beamwidth," Naval Res. Lab., Washington, DC, USA, RL Rep. 8841, 1984.

[13] J. K. Hsiao, "Design of error tolerance of a phased array," *Electron. Lett.*, vol. 21, no. 19, p. 834, 1985.

[14] P. D. Kaplan, "Predicting antenna sidelobe performance," *Microw. J.*, vol. 29, no. 9, pp. 201–204, 1986.

[15] M. I. Skolnik, "Nonuniform arrays," in *Antenna Theory*, R. E. Collin and F. Zucker, Eds. New York, NY, USA: McGraw-Hill, 1969.

[16] Y. Lo, "A mathematical theory of antenna arrays with randomly spaced elements," *IEEE Trans. Antennas Propag.*, vol. AP-12, no. 3, pp. 257–268, May 1964.

[17] Y. T. Lo, "A probabilistic approach to the problem of large antenna arrays," *J. Res. Nat. Bur. Standards D, Radio Sci.*, vol. 68D, no. 9, p. 1011, Sep. 1964.

[18] A. K. Bhattacharyya, *Phased Array Antennas: Floquet Analysis, Synthesis, BFNs and Active Array Systems*, 1st ed. Hoboken, NJ, USA: Wiley, 2006.

[19] Y. S. Shifrin and L. G. Kornienko, "The state-of-the-art of the statistical theory of antenna arrays," in *Proc. 6th Int. Symp. Antennas, Propag. EM Theory*, 2003, pp. 176–181.

[20] Y. S. Shifrin, "Pioneer award: Statistical antenna theory: Formation and extension," *IEEE Aerosp. Electron. Syst. Mag.*, vol. 31, no. 8, pp. 24–36, Aug. 2016.

[21] Y. Zhang, D. Zhao, Q. Wang, Z. Long, and X. Shen, "Tolerance analysis of antenna array pattern and array synthesis in the presence of excitation errors," *Int. J. Antennas Propag.*, vol. 2017, pp. 1–6, Jan. 2017.

[22] A. Schiessl, A. Genghammer, S. S. Ahmed, and L.-P. Schmidt, "Hardware realization of a 2 m×1 m fully electronic real-time mm-wave imaging system," in *Proc. Eur. Conf. Synth. Aperture Radar*, Nuremberg, Germany, Apr. 2012, pp. 40–s43.

[23] A. Schiessl, A. Genghammer, S. S. Ahmed, and L.-P. Schmidt, "Phase error sensitivity in multistatic microwave imaging systems," in *Proc. Eur. Microw. Conf.*, Oct. 2013, pp. 1631–1634.

[24] V. R. Gowda, M. F. Imani, T. Sleasman, O. Yurduseven, and D. R. Smith, "Focusing microwaves in the Fresnel zone with a cavity-backed holographic metasurface," *IEEE Access*, vol. 6, pp. 12815–12824, 2018.

[25] M. Wang, L. Crocco, S. Costanzo, R. Scapaticci, and M. Cavagnaro, "A compact slot-loaded antipodal Vivaldi antenna for a microwave imaging system to monitor liver microwave thermal ablation," *IEEE Open J. Antennas Propag.*, vol. 3, pp. 700–708, 2022.

[26] G. Yildiz, T. Yilmaz, and I. Akduman, "Rotationally adjustable hyperthermia applicators: A computational comparative study of circular and linear array applicators," *Diagnostics*, vol. 12, no. 11, p. 2677, Nov. 2022, doi: 10.3390/diagnostics12112677.

[27] Z. Chen, H. Sun, and W. Geyi, "Maximum wireless power transfer to the implantable device in the radiative near field," *IEEE Antennas Wireless Propag. Lett.*, vol. 16, pp. 1780–1783, 2017.

[28] B. J. DeLong, A. Kiourti, and J. L. Volakis, "A radiating near-field patch rectenna for wireless power transfer to medical implants at 2.4 GHz," *IEEE J. Electromagn., RF Microw. Med. Biol.*, vol. 2, no. 1, pp. 64–69, Mar. 2018.

[29] S. A. A. Shah and H. Yoo, "Radiative near-field wireless power transfer to scalp-implantable biotelemetric device," *IEEE Trans. Microw. Theory Techn.*, vol. 68, no. 7, pp. 2944–2953, Jul. 2020.

[30] T. Shaw and D. Mitra, "Metasurface-based radiative near-field wireless power transfer system for implantable medical devices," *IET Microw., Antennas Propag.*, vol. 13, no. 12, pp. 1974–1982, Oct. 2019.

[31] P. R. Stauffer, F. Rossetto, M. Leoncini, and G. B. Gentilli, "Radiation patterns of dual concentric conductor microstrip antennas for superficial hyperthermia," *IEEE Trans. Biomed. Eng.*, vol. 45, no. 5, pp. 605–612, May 1998.

[32] P. R. Stauffer, D. Neuman, C. Hwang, F. Rossetto, and C. J. Diederich, "Microwave vest for hyperthermia treatment of large area superficial disease," in *Proc. 1st Joint BMES/EMBS Conf. IEEE Eng. Med. Biol. 21st Annu. Conf. Annu. Fall Meeting Biomed. Eng. Soc.*, vol. 2, Oct. 1999, p. 1275.

[33] H. D. Trefná et al., "Quality assurance guidelines for superficial hyperthermia clinical trials," *Strahlentherapie Onkologie*, vol. 193, no. 5, pp. 351–366, 2017.

[34] S. P. Singh, "Microwave applicators for hyperthermia treatment of cancer: An overview," in *Proc. 3rd Int. Conf. Microw. Photon. (ICMAP)*, Dhanbad, India, Feb. 2018, pp. 1–3, doi: 10.1109/ICMAP.2018.8354467.

[35] G. Buonanno and R. Solimene, "Generalised random binned antenna arrays," *Prog. Electromagn. Res. C*, vol. 78, pp. 129–143, 2017.

[36] G. Buonanno and R. Solimene, "Unequally-excited linear totally random antenna arrays for multi-beam patterns," *IET Microw., Antennas Propag.*, vol. 12, no. 10, pp. 1671–1678, Aug. 2018.

[37] G. Buonanno and R. Solimene, "Comparing different schemes for random arrays," *Prog. Electromagn. Res. B*, vol. 71, pp. 107–118, 2016.

[38] G. Buonanno, S. Costanzo, and R. Solimene, "Broadband statistically designed thinned-binned array antennas," *IEEE Trans. Antennas Propag.*, vol. 71, no. 3, pp. 2454–2466, Mar. 2023.

[39] M. Skolnik, J. Sherman, III, and F. Ogg Jr., "Statistically designed density-tapered arrays," *IEEE Trans. Antennas Propag.*, vol. AP-12, no. 4, pp. 408–417, Jul. 1964.

[40] Y. T. Lo, "Random periodic arrays," *Radio Sci.*, vol. 3, no. 5, pp. 425–436, May 1968.

[41] G. Buonanno and R. Solimene, "Global characterization of linear statistically thinned antenna arrays," *IEEE Access*, vol. 9, pp. 119629–119640, 2021.

[42] K. Buchanan, O. Sternberg, S. Wheeland, and J. Rockway, "Examination of the near field response of circular antenna arrays," in *Proc. United States Nat. Committee URSI Nat. Radio Sci. Meeting (USNC-URSI NRSM)*, Jan. 2017, pp. 1–2.

[43] W. Feller, *An Introduction to Probability Theory and its Applications*, vol. 2. New York, NY, USA: Wiley, 1966.

[44] M. Zelen and N. C. Severo, "Probability functions," in *Handbook of Mathematical Functions With Formulas, Graphs, and Mathematical Tables* (National Bureau of Standards Applied Mathematics Series), M. Abramowitz and I. A. Stegun, Eds. Dec. 1972.

[45] M. Bensimhoun, "N-dimensional cumulative function, and other useful facts about Gaussians and normal densities," Jerusalem, Israel, Tech. Rep., 2009.

[46] C. Mallows, "Another comment on O'Cinneide," *Amer. Statistician*, vol. 45, no. 3, p. 257, Aug. 1991.

[47] D. Gilat and T. P. Hill, "Quantile-locating functions and the distance between the mean and quantiles," *Statistica Neerlandica*, vol. 47, no. 4, pp. 279–283, Dec. 1993.

[48] G. Buonanno and R. Solimene, "Large linear random symmetric arrays," *Prog. Electromagn. Res. M*, vol. 52, pp. 67–77, 2016.

[49] A. Nuttall, "Some integrals involving the Q_M function (corresp.)," *IEEE Trans. Inf. Theory*, vol. IT-21, no. 1, pp. 95–96, Jan. 1975.

Giovanni Buonanno (Member, IEEE) received the M.S. degree (summa cum laude) in electronic engineering from Seconda Università degli Studi di Naples (SUN), Aversa, Italy, in 2014, and the Ph.D. degree in industrial and information engineering from the University of Campania, Caserta, Italy, in 2018.

Then, he joined the Research Group in Applied Electromagnetics, SUN. He defending the Ph.D. thesis, in January 2019. He is currently a Research Fellow with the University of Calabria, Rende, Italy. His research interests include analysis and design of nonuniformly-spaced antenna arrays, biomedical applications, signal processing, and machine learning.

Sandra Costanzo (Senior Member, IEEE) received the Laurea degree (summa cum laude) in computer engineering from the Università della Calabria, Rende, Italy, in 1996, and the Ph.D. degree in electronic engineering from the Università Mediterranea di Reggio Calabria, Reggio Calabria, Italy, in 2000.

Since 2019, she has been an Associate with the Institute for Electromagnetic Sensing of the Environment-National Research Council of Italy (IREA-CNR), Naples, Italy. She is currently an Associate Professor with the Università della Calabria, where she is the Coordinator of master's degree in telecommunication engineering and the Rector's Delegate for Health Safety. She teaches courses on electromagnetic waves propagation, antennas, remote sensing, radar, sensors, and electromagnetic diagnostics. She has authored or coauthored over 200 contributions in international journals, books, and conferences. Her research interests are focused on near-field/far-field techniques, antenna measurement techniques, antenna analysis and synthesis, numerical methods in electromagnetics, millimeter wave antennas, reflectarrays, synthesis methods for microwave structures, electromagnetic characterization of materials, biomedical applications, and radar technologies.

Dr. Costanzo is a member of the IEEE MTT-28 Biological Effects and Medical Applications Committee, IEEE South Italy Geoscience and Remote Sensing Ear, Consorzio Nazionale Interuniversitario per le Telecomunicazioni (CNIT), Società Italiana di Elettromagnetismo (SIEM), and Centro Interuniversitario sulle Interazioni fra Campi Elettromagnetici e Biosistemi (ICEMB). She is a Board Member of the IEEE AP/ED/MTT North Italy Chapter. She received the Telecom Prize for the Best Laurea Thesis, in 1996, and the 2013 Best Academia and Research Application in Aerospace and Defense Award for the Application Software Defined Radar Using the NI USRP 2920 Platform. In 2017, she was awarded the Italian National Scientific Qualification for the Full Professor position. She is an Associate Editor of IEEE ACCESS, IEEE JOURNAL OF ELECTROMAGNETICS, RF AND MICROWAVES IN MEDICINE AND BIOLOGY, and ELECTRONICS (section "Microwave and Wireless Communications"). She is an Editorial Board Member of *Radioengineering and International Journal of RF and Microwave Computer-Aided Engineering*. She is an Editor of the books *Microwave Materials Characterization* (INTECH, 2012) and *Wave Propagation Concepts for Near-Future Telecommunication Systems*' (INTECH, 2017). She was the Lead Editor of the Special Issues on *Reflectarray Antennas: Analysis and Synthesis Techniques*, in 2012, *Advances in Radar Technologies*, in 2013, COMPRESSED SENSING: APPLICATIONS IN RADAR AND COMMUNICATIONS, in 2016, *Bioengineering Applications of Electromagnetic Wave Propagation*, in 2019, and *Microwave Sensors for Biomedical Applications*, in 2020.

Open Access funding provided by 'Università della Calabria' within the CRUI CARE Agreement